

Sequential clustering of star formation in IC 1396

Ya Fang Huang and Jin Zeng Li

National Astronomical Observatories, Chinese Academy of Sciences, Beijing 100012, China;
huangyf@nao.cas.cn

Received [year] [month] [day]; accepted [year] [month] [day]

Abstract We present in this paper a comprehensive study of the H II region IC 1396 and its star formation activity, in which multi-wavelength data ranging from the optical to the near- and far-infrared were employed. The surface density distribution of all the 2MASS sources with certain detection toward IC 1396 indicates the existence of a compact cluster spatially consistent with the position of the exciting source of the H II region, HD 206267. The spatial distribution of the infrared excessive emission sources selected based on archived 2MASS data reveals the existence of four sub-clusters in this region. One is in association with the open cluster Trumpler 37. The other three are found to be spatially coincident with the bright rims of the H II region. All the excessive emission sources in the near infrared are cross-identified with the AKARI IRC data, an analysis of the spectral energy distributions (SEDs) of the resultant sample leads to the identification of 8 CLASS I, 15 CLASS II and 15 CLASS III sources in IC 1396. Optical identification of the sample sources with R magnitudes brighter than 17 mag corroborates the results from the SED analysis. Based on the spatial distribution of the infrared young stellar objects at different evolutionary stages, the surrounding sub-clusters located in the bright rims are believed to be younger than the central one. This is consistent with a scenario of sequential star formation in this region. Imaging data of a dark patch in IC 1396 by Herschel SPIRE, on the other hand, indicate the presence of two far-infrared cores in LDN 1111, which are likely new generation protostellar objects in formation. So we infer that the star formation process in this H II region was not continuous but episodic.

Key words: techniques: photometric — stars: formation — stars: pre-main sequence — infrared: stars

1 INTRODUCTION

Molecular clouds (Lada & Lada, 2003) are essential sites of clustered star formation and the formation of massive stars. Cepheus OB2 (Cep OB2), known to be located in the local (Orion) spiral arm, is divided into two subgroups (Simonson, 1968): 1) Cep OB2a contains 75 O- and B-stars that spread over a large area, between $100^\circ < l < 106^\circ$ and $+2^\circ < b < +8^\circ$. It has an estimated age of 6-7 million years; 2) Cep OB2b, namely Trumpler 37 (Tr 37), has an age of 3 million years and is among the youngest known open clusters (Kun et al., 2008).

Tr 37 is associated with the shell-like H II region, IC 1396. IC 1396 is located at the southwest tip of Cep OB2, just above the galactic plane at $l = 99.3^\circ$ and $b = 3.74^\circ$. This H II region is mainly excited by the central O6 star HD 206267. As an extended H II region ($\sim 3^\circ$) at about 800 pc (Simonson, 1968), it harbors a significant population of Pre-Main Sequence stars (PMS) with low- to intermediate masses.

Large-scale observations of IC 1396 with rotational CO lines (Patel et al., 1995; Weikard et al., 1996) and the radio map (Matthews et al., 1980; Wendker & Baars, 1980) have uncovered a ring-like

and scattered structure. The appearance of the H II region is dominated by a high degree of fragmentation into many dark and bright-rimmed globules. Near-infrared (IR) observations of IC 1396 and extinction maps obtained from Two Micron All Sky Survey (2MASS) data reveal star-formation activity and large numbers of globules in this region (Froebrich et al., 2005). Some of the densest regions in IC 1396 have already been investigated in detail (IC 1396N: Neri et al. (2007); Choudhury et al. (2010); Getman et al. (2007). IC 1396W: Froebrich & Scholz (2003). IC 1396A: Reach et al. (2004, 2009)). More and more young stellar objects (YSOs) have been detected with CHANDRA, SPITZER and other bands (Mercer et al., 2009; Barentsen et al., 2011; Nakano et al., 2012).

The pioneering InfraRed Astronomical Satellite (IRAS) all-sky survey covers more than 96% of the entire sky in four photometric bands at 12, 25, 60 and 100 μm . The IRAS Sky Survey Atlas (ISSA) has shown that mid- and far-IR census is essential for studying the dust embedded objects in IC 1396. 2MASS is the first near-IR survey that made uniformly calibrated observations of the entire sky in the J (1.25 μm), H (1.65 μm), and K_S (2.16 μm) bands with a pixel size of $2''.0$. Sources brighter than about 1 mJy in each band were detected with a signal-to-noise ratio greater than 10, which leads to a photometric completeness to 15.9, 15.0, and 14.3 mag, respectively, for each band in unconfused regions. For details about the 2MASS survey and the 2MASS Point Source Catalog (PSC), please consult the 2MASS Explanatory Supplement¹.

Near-IR large area surveys and 2MASS provide an opportunity to investigate the sources with excessive emission, but their mid- and far-IR counterparts are rare and are hard to be uniquely identified in the IRAS catalogue, preventing an efficient search of objects surrounded by dust. AKARI, a satellite operated by Japan, fulfills the need for a new mid- and far-IR whole sky survey with better sensitivity and higher spatial resolution. Since its launch on 2006 February 21, AKARI has mapped 96% of the entire sky in mid and far-IR using two instruments on board: the InfraRed Camera (IRC; Onaka et al., 2007) and Far-Infrared Surveyor (FIS; Kawada et al., 2007). The FIS swept about 94% of the whole sky more than twice at 65, 90, 140, and 160 μm wavebands, while IRC swept more than 90% of the whole sky more than twice using two filter bands centered at 9 μm ($S9W$, 7 - 12 μm) and 18 μm ($L18W$, 14 - 25 μm) (Ishihara et al., 2010).

Most young stellar objects (YSOs) present an IR excess, which is interpreted in terms of the presence of a circumstellar disk. We focus on the spatial distribution of the sources with excessive emission and try to elucidate the mode of star formation in IC 1396. This paper is organized as follows. We present in Section 2 the retrieval of the archived 2MASS and AKARI data, optical spectroscopy and its data reduction. In Section 3, we present how we explored the four subclusters spatially coincident with the bright rims of IC 1396. Optical identification and SED classification of the sample sources follows in Section 4. The results achieved are discussed in Section 5 and summarized in Section 6.

2 DATA ACQUISITION AND ANALYSIS

2.1 Archival Data

Archived data from the 2MASS PSC were used in this work. To guarantee the reliability of the data, we employed the following strict requirements in the sample selection, which are revised based on the criteria presented by Li & Smith (2005): 1) The photometric uncertainties for each extracted 2MASS point source should be less than or equal to 0.1 mag at all three bands ($[JHK_S]_{-cmsig} \leq 0.1$). 2) Only sources with a K_S -band signal-to-noise ratio above 15 are selected.

The sample of excessive emission sources selected based on the 2MASS data is cross-identified with the AKARI (ASTRO-F) IRC PSC² using the simple positional correlation method. Only sources with valid $S9W$ data (fQual.09 equals to 3) were considered. Based on the statistical result of the relationship between the positional offset and the numbers of counterparts both detected with the AKARI IRC PSC and 2MASS PSC, we found the chance of false matches becomes large when the tolerance radius is larger than $3''$. So a positional tolerance of $3''$ is adopted. If more than one AKARI source are found

¹ <http://www.ipac.caltech.edu/2mass/releases/allsky/doc/explsup.html>

² <http://darts.isas.jaxa.jp/astro/akari/cas.html>

within the tolerance radius, only the closest one is adopted. The flux of the IRC PSC sources were then converted to apparent magnitude with the following equation:

$$m = -2.5 \times \log_{10}\left(\frac{Flux}{Flux_0}\right)$$

where $Flux_0$ (zero magnitude flux) is 56.262 ± 0.8214 Jy and 12.00 ± 0.1751 Jy for $9 \mu m$ and $18 \mu m$ bands, respectively.

2.2 Optical Spectroscopy

Spectroscopic observations of all the sample sources in IC 1396 with USNO R magnitudes brighter than 17.0 were undertaken on the 2.16 m optical telescope of the National Astronomical Observatories of the Chinese Academy of Sciences (NAOC). The OMR (Optomechanics Research Inc.) and the detector PI 1340×400 CCD were used in both runs of observations. The low-resolution spectroscopy (with dispersion of 200 \AA mm^{-1} , $4.8 \text{ \AA pixel}^{-1}$, and $2''.5$ slit) centered at 6300 \AA has been carried out on September 12, December 11, 2009, and October 3 to 4, 2010.

The spectral data were reduced following standard procedures in the NOAO Image Reduction and Analysis Facility (IRAF, version 2.11) software packages. The CCD reduction includes bias and flat-field correction, nebular and sky background subtraction, and cosmic ray removal. Wavelength calibration was performed based on Helium-Argon lamps exposed at both the beginning and the end of the observations each night. Flux calibration of each spectrum was conducted based on observations of at least two of the KPNO spectral standards (Massey et al., 1988) each night. The atmospheric extinction is corrected by the mean extinction coefficients measured for the Xing-Long Station, where the 2.16m telescope is located, by the Beijing-Arizona-Taiwan-Connecticut (BATC) multicolor survey.

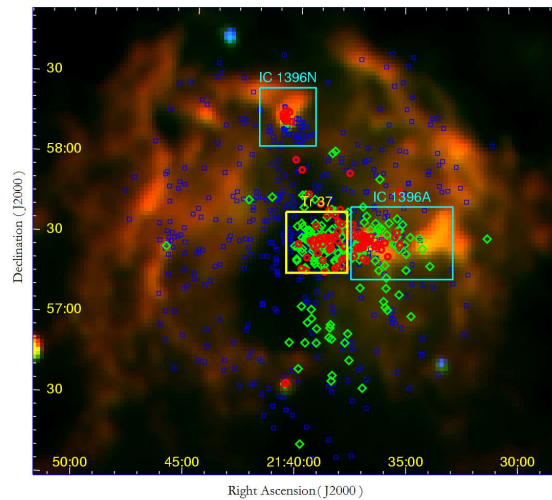


Fig. 1 Distribution of known YSOs in IC 1396. Historical studies were limited to the densest parts: IC 1396A, IC 1396N and Tr 37. Red circles indicate weak-line T Tauri stars and CLASS II/III sources, while green diamonds indicate classical T Tauri stars and CLASS I sources. The background image is a trichromatic image generated from IRAS 25 (blue), 60 (green), and 100 (red) μm maps.

3 CLUSTERING OF STAR FORMATION IN IC 1396

Historical studies revealed the existence of many YSO candidates and most of them are found to be congregated to the densest parts of IC 1396. Figure 1 shows the distribution of YSOs in the literature as mentioned in Section 1. Its border shows the region studied in this paper. It extends from 21^h28^m to 21^h52^m in right ascension and from 56° to 59° in declination, centered on R.A. = $21^h40^m00^s$, Dec = $57^\circ30'00''$ (J2000.0), which is believed to encompass all the compact subclusters to their full extent.

3.1 Color-color Diagram

The 2MASS database contains more than half a million photometric detections in this region. We narrowed down the catalogue to 108,966 sources using our select criteria mentioned above.

2MASS JHK_S color-color (C-C) diagram is widely used to select sources with IR excessive emissions. Figure 2 shows the C-C diagram for IC 1396. All the 2MASS sources that match our criteria are put into the JHK_S C-C diagram and denoted as dots. We define 598 objects as YSO candidates whose colors place them below the right line of the normal star reddening band and $H - K_S > 0.5$. Those sources are selected for they possess intrinsic color excesses likely originating from emission of circumstellar dust, commensurate with their embedded nature. The color distinction helps to eliminate foreground field stars and narrowed the YSO candidates sample.

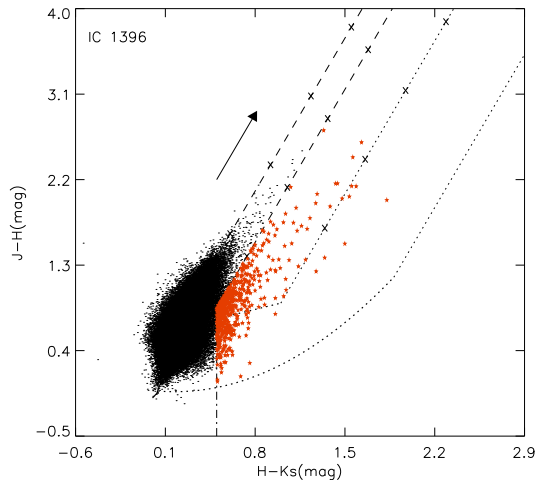


Fig. 2 ($J - H$) vs. ($H - K_S$) C-C diagram of IC 1396. The sample sources are denoted as dots. Selected IR excessive emission sources are labeled in red. Black solid lines represent the loci of the MS dwarfs and giant stars (Bessell & Brett, 1988). Two paralleled dashed lines define the reddening band for normal stars. The arrow shows a reddening vector of $A_v = 5$ mag (Rieke & Lebofsky, 1985). The left dotted line indicates the locus of dereddened T Tauri star (Meyer et al., 1997) and its reddening band boundary. The right dotted line indicates the locus of dereddened HAeBe (Lada & Adams, 1992) and its reddening direction. Crosses were over plotted with an interval corresponding to 5 mag of visual extinction.

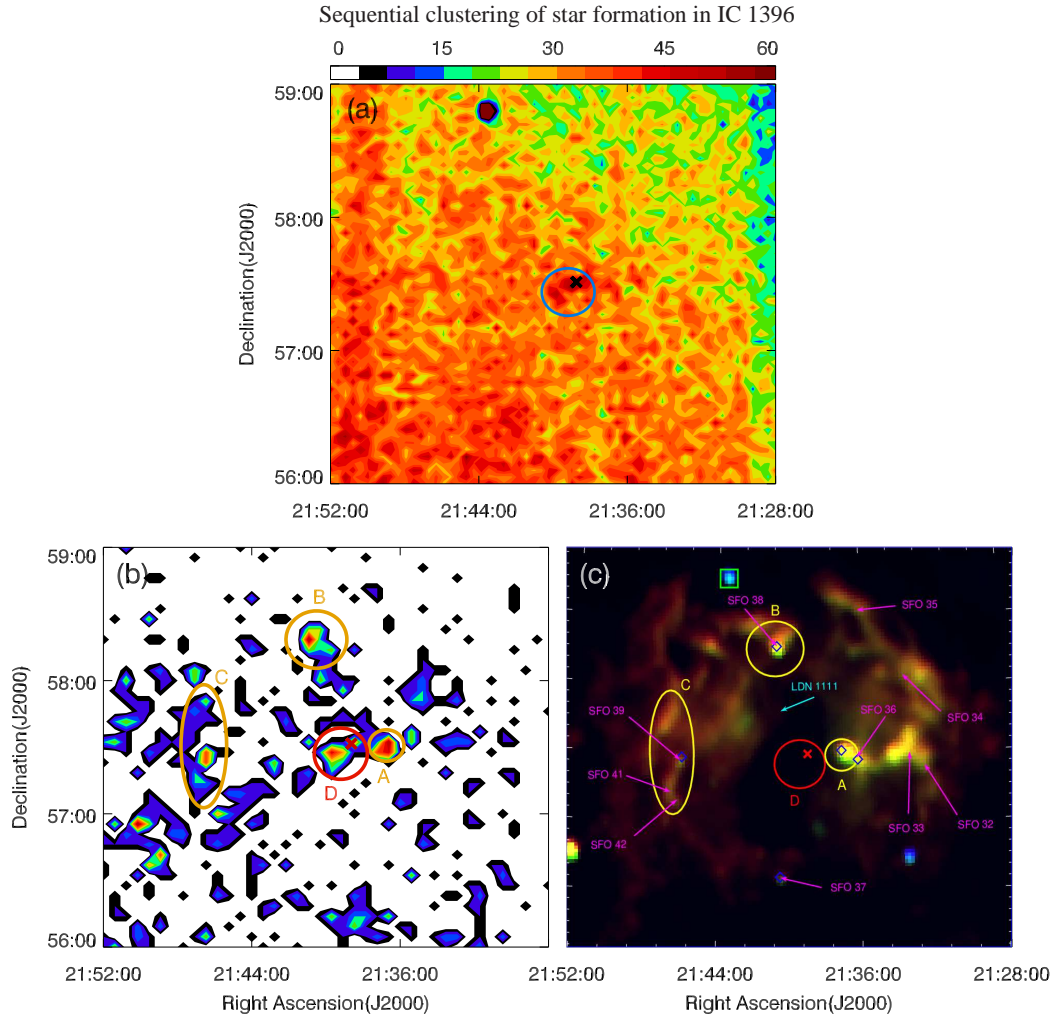


Fig. 3 (a) Surface density distribution of the 2MASS sources toward IC 1396. The densest region at the center marked with circle is consistent with the position of the open cluster Tr 37, and the cross indicates HD 206267 (R.A. = $21^h38^m57^s$, decl. = $+57^\circ29'20''$ (J2000)). The hole on the top left corner is formed for a saturated bright source, which is marked with green box in panel (c). The color bar indicates the number of sources in every 0.0025 square degrees. (b) Spatial distribution for 598 2MASS excessive emission sources. Red cross indicates the exciting star HD 206267. Yellow circles mark the four densest regions of YSO candidates, which harbor active star formation. (c) Trichromatic image of IC 1396 generated from IRAS 25 (blue), 60 (green), and 100 (red) μm maps. Bright rims (Sugitani et al., 1991) and BOLOCAM data (blue diamonds) are plotted. Red cross indicates the main exciting source HD 206267.

3.2 Surface Density Distribution

The spatial distribution of all the 2MASS sources and YSO candidates are presented in Figure 3. On the scale of the entire IC 1396, significant stellar density enhancement in the center region is easily distinguished in the stellar surface density distribution of all the 2MASS sources (in Figure 3 (a)). There are about 59 sources in 0.0025 deg^2 at the densest region, which coincides with the young open cluster Tr 37. But we can't find the structure of the H II region in this panel.

In panel (b), the spatial distribution of the YSO candidates, there are four densest regions revealed. Compared with the $100\ \mu\text{m}$ image from IRAS, the A, B, C subclusters correspond to the bright rims (Sugitani et al., 1991) marked in Figure 3 (c), while the central subcluster D is at the location of open cluster Tr 37. Otherwise, region A and region B correspond to IC 1396 A and IC 1396 N, centered at $21^{\text{h}}36^{\text{m}}54^{\text{s}}, 57^{\circ}33'00''$ (J2000.0) and $21^{\text{h}}40^{\text{m}}42^{\text{s}}, 58^{\circ}15'14''$ (J2000.0), respectively. Region C is the most scattered one, and contains several stellar aggregates. Among them the most compact and biggest one is centered at $21^{\text{h}}46^{\text{m}}15^{\text{s}}, 57^{\circ}25'00''$ (J2000.0). Compared to the outer regions A, B, and C, region D is hardly to be found in ISSA image, because it has already lost dust protection in IR bands for the radiation of the exciting star HD 206267. But it still contains a number of YSO candidates.

4 IDENTIFICATION AND CLASSIFICATION OF EXCESSIVE EMISSION SOURCES IN IC 1396

To further investigate the scenario of star formation in IC 1396, AKARI IRC PSC was employed. Mid-IR data are more sensitive to cold dusts in the circumstellar disks and are essential for SED fitting. All the excessive emission sources selected based on the 2MASS C-C diagram were cross-identified with the AKARI IRC PSC, which resulted in a sample of 44 sources. Except 4 classical Be stars (CBe) and 2 Carbon stars identified with SIMBAD, all of the sample sources are presented in Table 1, which presents the sequences number of these sources, 2MASS PSC coordinates (J2000), USNO V magnitudes, $\text{EW}[\text{H}\alpha]$, $\text{EW}[\text{Li}]$, spectral types, and the classification based on SEDs.

4.1 Optical identification

To identify and classify the sample sources, optical spectra were obtained with the 2.16 m optical telescope of the NAOC. Combined with equivalent width measurements of $\text{H}\alpha$ ($\text{EW}[\text{H}\alpha]$), all the sources with spectral types earlier than F5 and $\text{H}\alpha$ in emission were identified as Herbig Ae/Be stars (HAeBe). Classical T Tauri stars (CTTS) are, on the other hand, selected based on the criteria that a CTTS shows $\text{EW}[\text{H}\alpha]$ value greater than $3\ \text{\AA}$ for K0 – K5 stars, $\text{EW}[\text{H}\alpha]$ value greater than $10\ \text{\AA}$ for K7 – M2.5 stars, $\text{EW}[\text{H}\alpha]$ value greater than $20\ \text{\AA}$ for M3 – M5.5 stars, and $\text{EW}[\text{H}\alpha]$ value greater than $40\ \text{\AA}$ for M6 – M7.5 stars (White & Basri, 2003). However, stars with values of $\text{EW}[\text{H}\alpha]$ below these levels are

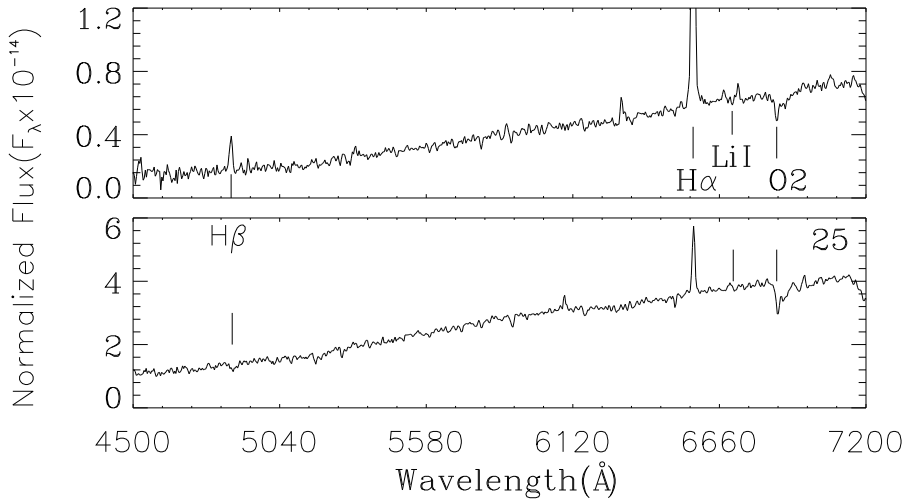


Fig. 4 Typical WTTS (No.21) and CTTS (No.25) spectra in IC 1396, showing the Balmer series in emission (mainly $\text{H}\alpha$) and Li absorption at $6707\ \text{\AA}$.

not necessarily weak-line T Tauri stars (WTTS) as they share very similar SEDs with MS stars. Further identification based on the detection of Li I 6707 Å absorption is necessary (Martín, 1998). Except 4 CBe, 23 stars out of the 33 observed sources are identified as YSOs due to the presence of prominent H α emission. Among these, there are 5 CTTS, 7 HAeBe, and 8 WTTS. For the left 3, no prominent Li I absorption is detected because of low Signal to Noise Ratio of the optical spectra. However, the existence of strong H α emission and excessive emission in IR seems to corroborate their nature as YSOs. Figure 4 illustrates the sample spectra of WTTS and CTTS, respectively. Among the sample of 33 observed sources, 27 were found to be strong H α emission stars. And 3 HAeBe, 1 CTTS and 13 WTTS are newly discovered in IC 1396.

4.2 Classification based on SED fitting

We tried to determine the evolutionary status of the sample sources based on their SEDs. A grid of 200,000 YSO models was developed (Robitaille et al., 2006), spanning a wide range of evolutionary stages for different stellar masses, to model the SED from optical to millimeter wavelengths. This archive transfer provides a linear regression tool which can select all model SEDs that fit the observed SED better than a specified χ^2 (Robitaille et al., 2006).

On the basis of the “four staged” star formation scenario proposed by Shu et al. (1987), Lada (1987) developed a widely used classification scheme for YSOs, primarily based on their SEDs. With an evolutionary sequence from early type to late type, YSOs were classified into Class I to III. Robitaille et al. (2006) presented a classification scheme that is essentially analogous to the class scheme, but refers to the actual evolutionary stage of the object based on physical properties like disk mass and envelope accretion rate. However, in view of the differences between observable and physical properties, ages fitted by the tool and the slope of its near/mid-IR SED are our primary reference standard. Class I refers to those objects that have $Age \approx 10^5$ yr and $Slope_{near/mid-IR} > 0$, Class II refers to $Age \approx 10^6$ yr and $Slope_{near/mid-IR} \leq 0$, and Class III is for objects whose SED is similar to a black-body spectrum.

Multi-wavelength online data are used for SED fitting. Besides 2MASS PSC and AKARI IRC/FIS data, we used: 1) BVR photometry from the Naval Observatory Merged Astrometric Dataset (NOMAD); 2) the mid-IR A (8.28 μm), C (12.13 μm) and D (14.65 μm) provided by the MSX6C IR PSC; 3) the far-IR IRAS Point Sources photometry at 12, 25, 60 and 100 μm ; 4) IRAC and MIPS photometry at 3.6, 4.5, 5.8, 8 and 24 μm for a handful of sources. As a result, we end up SED fitting with a photometric catalogue with large wavelength coverage. Though several sources lack data at far-IR bands, it is still crucial to investigate the PMS nature of sample sources in terms of IR excess in their SEDs.

The evolutionary status of all the YSO candidates listed in Table 1 further confirmed by results of the SED fitting. Figure 5 illustrates the SED of the CLASS I and CLASS II sources of the sample. Based on the SED fitting, all the sample sources indicate masses of $< 5 M_{\odot}$ and ages of < 3 Myr, which is in good accordance with the results of Nakano et al. (2012) and Choudhury et al. (2010).

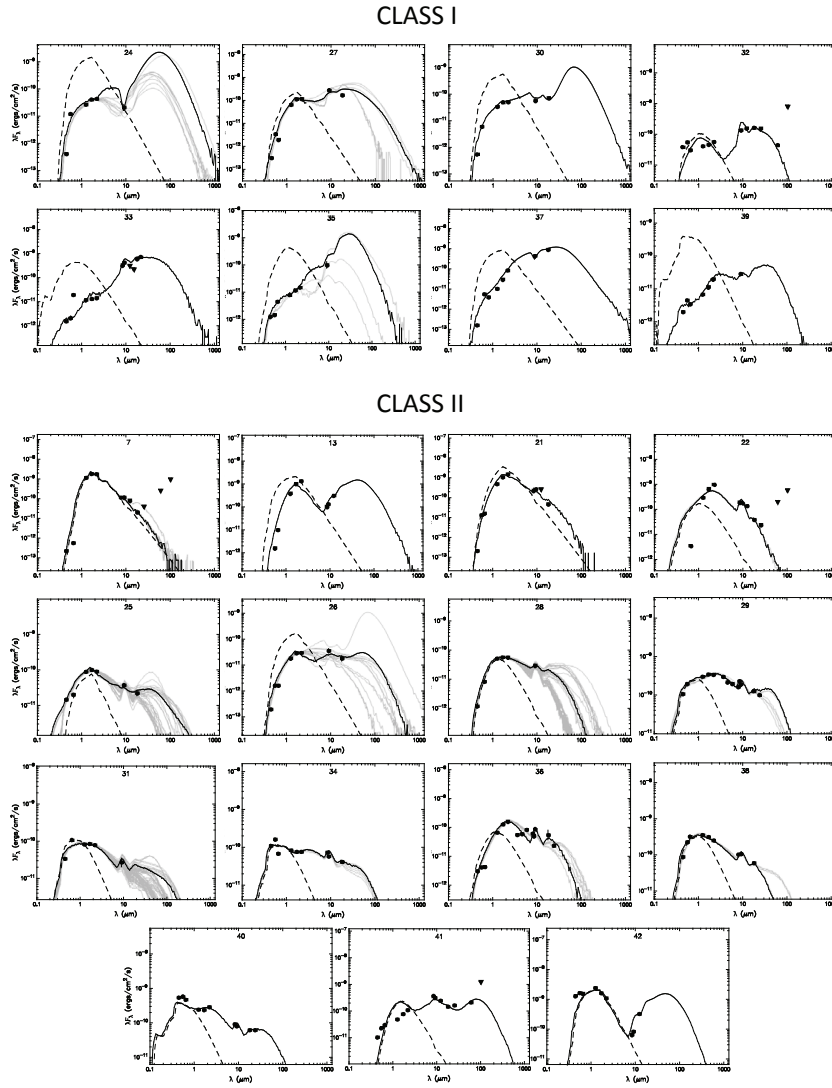


Fig. 5 Results of the SED fitting for the sample sources. The solid black curve gives the best model fitting of the data points with the smallest χ^2 . The gray curves represent the other potential model fitting results with $\chi^2/N - \chi_{best}^2/N < 3$. The dashed curve indicates the photosphere that is used as input for the radiative transfer code. The black dots show the measured fluxes currently available. The filled upside-down triangles indicate upper limit detection in each of the corresponding bands.

Table 1: Optical identification and classification of the sample sources toward IC 1396.

ID	R.A.		Dec.		V [mag]	EW		Sp.	Class		
	J2000					[H α]	[Li]		Spectra	C-C diagrams	SEDs
1*	21 42 33.57	58 14 39.11	12.21	-12.1	...	B2	CBe	CBe	...		
2*	21 48 21.16	56 09 20.15	12.41	-9.05	...	B4	CBe	CBe	...		
3*	21 36 59.63	58 08 24.72	12.21	-27.9	...	B3	CBe	CBe	...		
4	21 42 24.16	57 44 09.96	14.77	-4.99	...	O9	CBe	CBe	...		
5	21 29 23.95	56 19 49.43	14.73	-2.15	0.57	M4	WTTS	WTTS	III		
6	21 47 15.45	56 23 45.95	15.63	-6.18	0.08	M4	WTTS	WTTS	III		
7	21 43 33.09	57 25 25.31	24.61	WTTS	II		
8	21 46 35.97	57 49 31.79	18.07	WTTS	III		
9*	21 43 08.73	57 11 58.20	16.1	-20.5	2.02	M7	WTTS	WTTS	III		
10*	21 34 15.59	56 18 11.88	16.1	-1.97	0.35	M6	WTTS	WTTS	III		
11*	21 40 03.86	57 42 18.71	17.41	M3	...	WTTS	III		
12*	21 45 34.12	56 23 42.72	16.81	M2	...	WTTS	III		
13*	21 32 44.54	56 21 25.56	16.1	-4.56	0.86	M7	WTTS	WTTS	II		
14	21 46 41.23	57 00 10.80	14.97	-3.38	0.48	M5	WTTS	WTTS	III		
15*	21 39 10.63	57 06 47.16	16.01	-2.36	0.53	M4	WTTS	WTTS	III		
16*	21 50 21.50	56 53 10.32	20.61	WTTS	III		
17	21 43 16.43	56 01 42.60	14.3	-10.2	...	M9	WTTS	WTTS	III		
18	21 42 47.61	58 57 20.52	13.11	M8	...	WTTS	III		
19	21 42 12.04	58 25 12.00	26.41	M8	...	WTTS	III		
20*	21 39 06.38	57 43 51.60	16.95	-14.1	...	M7	WTTS	WTTS	III		
21	21 38 42.31	57 30 27.71	16.41	-12.9	...	M4	WTTS	WTTS	II		
22	21 39 09.33	58 38 53.87	16.41	M7	...	WTTS	II		
23*	21 43 51.47	58 15 07.92	19.73	WTTS	III		
24*	21 48 11.75	57 59 41.64	15.7	-86.3	0.84	F8	CTTS	CTTS	I		
25	21 36 49.56	57 48 23.39	14.85	-6.52	0.02	G6	CTTS	CTTS	II		
26	21 45 05.87	57 11 38.75	18.21	CTTS	II		
27	21 34 19.63	57 30 02.52	15.7	-45.1	0.23	F7	CTTS	CTTS	I		
28	21 35 43.60	57 03 47.52	14.81	-2.92	0.23	K3	WTTS	CTTS	II		
29* ¹	21 38 17.32	57 31 22.07	13	-14.5	0.11	F9	CTTS	CTTS	II		
30	21 46 00.26	57 23 09.60	18.35	CTTS	I		
31	21 45 54.07	57 28 18.48	14.4	-9.65	0.1	K4	CTTS	CTTS	II		
32	21 30 22.84	58 28 51.95	14.37	-40.5	0.31	A9	HAeBe	HAeBe	I		
33	21 49 38.27	56 54 36.72	15.7	-141	0.12	F2	HAeBe	HAeBe	I		
34	21 35 19.15	57 36 38.15	15.21	-6.98	0.01	A8	HAeBe	HAeBe	II		
35*	21 29 58.03	56 28 50.51	17.5	HAeBe	I		
36 ²	21 36 39.14	57 29 53.16	17	HAeBe	II		
37	21 46 07.12	57 26 31.91	17.21	HAeBe	I		
38	21 45 02.32	56 49 51.60	14.21	2.35	0.25	F9	...	HAeBe	II		
39	21 45 24.55	57 55 49.08	16.1	-11.1	0.79	F3	HAeBe	HAeBe	I		
40	21 38 08.44	57 26 47.75	14.15	-5	0.1	A2	HAeBe	HAeBe	II		
41	21 33 17.78	57 48 13.31	14.53	-62.6	0.13	F3	HAeBe	HAeBe	II		
42	21 51 00.57	56 21 19.44	10.24	-43.1	...	F3	HAeBe	HAeBe	II		
43	21 43 56.92	58 35 45.95	18.17	Carb.	...		
44	21 38 28.34	57 08 19.32	16.91	M7	...	Carb.	...		

* Sources not detected with IRC 18 μm ¹ IC 1396 A: θ – identified as CTTS from Sicilia-Aguilar et al. (2006).² Identified as CLASS II source from Reach et al. (2009).

5 DISCUSSION

Marschall et al. (1990) suggested that stars of the first generation in IC 1396 reached the main sequence at 7 Myr ago, and Sicilia-Aguilar et al. (2005) gave an age of 4 Myr for the young open cluster Tr 37 based on optical photometry and theoretical isochrones. The expansion of the H II region has created a swept-up shell and resulted in a compressed molecular ring around its periphery (Nakano et al., 2012). Based on the physical scale of the ring, Patel et al. (1995) suggested a dynamical age of 2 – 3 Myr. A number of H α stars with ages younger than 3 Myr were detected by Nakano et al. (2012). They are spatially associated with the bright rims. Based on the disparity of ages for various groups of stars, we tentatively suggest a scenario of sequential or episodic star formation in IC 1396.

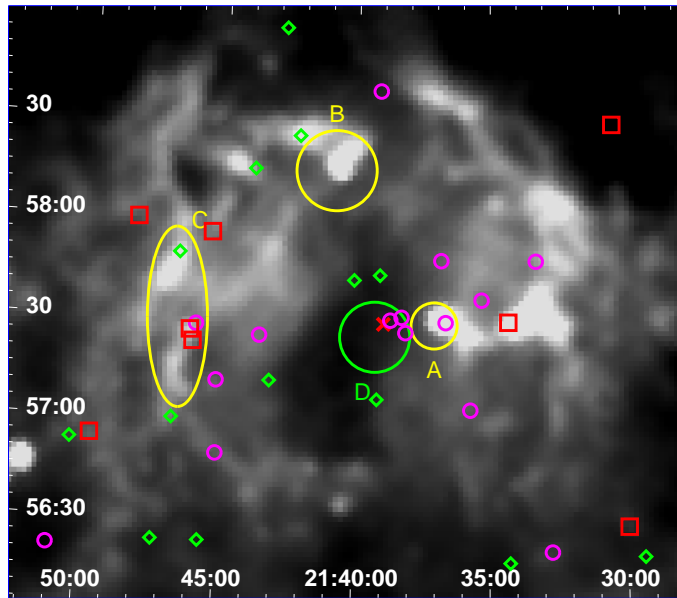


Fig. 6 Distribution of the sample sources classified with SEDs. CLASS I, II, and III sources are indicated with red boxes, magenta circles, and green diamonds, respectively. The red cross represents the exciting star HD 206267. The background image is the IRAS 100 μ m map of IC 1396

In this work, we provide new additional evidence to support a scenario of sequential or episodic formation of stellar clusters in IC 1396. Figure 6 presents the IRAS 100 μ m mosaic of IC 1396, on which the sample sources classified based on SEDs are overlaid with different symbols. Although the number of Class I sources identified in this study is small, all the CLASS I sources are found to be located in the bright rims or the molecular ring of IC 1396, while YSOs at later evolutionary stages (e.g. CLASS III) are congregated to the central part of the H II region. Furthermore, all the identified CLASS I and CLASS II sources are located in the surrounding sub-clusters rather than the central open cluster Tr 37. All these are consistent with an episodic nature of star and cluster formation in this H II region. A direct consequence of episodic star formation is that different generations of stars occupy distinct territories.

A spatial gap seems to exist between the central open cluster and the surrounding subclusters in both the optical and the near-IR, which is believed to be the results of discontinuous star formation in this region. To further investigate the interstellar materials within the gap, Herschel SPIRE data were

employed. As shown in Figure 3 (c), there is an optically dark cloud between Tr 37 and subcluster B. This dark cloud was catalogued by Lynds (1962) as LND 1111, which is highly extinct both in the optical and the near-IR. The right panel of Figure 7 presents a composite image of LND 1111, which was compiled with the SPIRE 250 μm (blue), 350 μm (green), and 500 μm (red) imaging data. It is evident that the dark globule corresponding to LND 1111 in the DSS-2 blue band image (left panel in Figure 7) is bright in emission in the far-IR. This indicates the existence of large amount cold dusts. The overlaid contours generated based on the Herschel SPIRE image indicate the presence of two far-IR cores, which are likely nurseries of new generation stars. Therefore, we infer that new generations of star formation is going on in IC 1396, and star formation in this region is not continuous but sequential or episodic. Further investigations are necessary to explore if new generations of star and cluster formation in IC 1396, both in the vacant bubble and the working interface of the HII region, has a triggered origin or not.

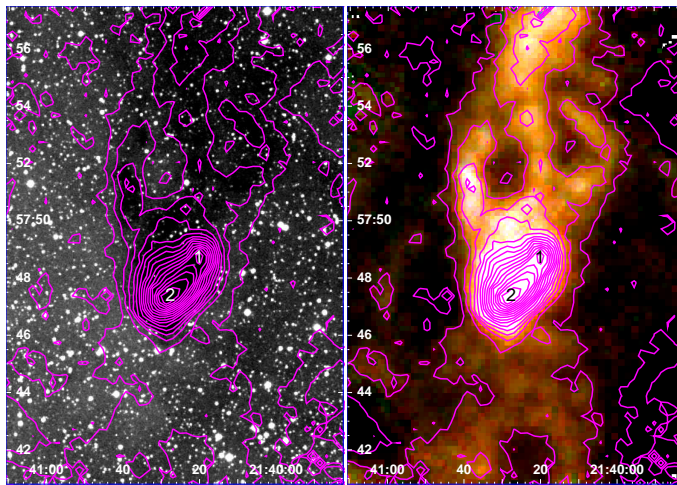


Fig. 7 Left: DSS 2 blue band image of LND 1111. Right: Color composite image of the dark cloud LND 1111 in 250 μm (blue), 350 μm (green) and 500 μm (red). Magenta contours in both two images are generated from the Herschel SPIRE image in 500 μm band.

6 SUMMARY

We present in this paper a comprehensive study of the H II region IC 1396 and its star formation activity. Excessive emission sources are selected based on the archived 2MASS data and their cross-identification with AKARI IRC PSC. SED fittings are employed to classify the IR sources. In the target region, 8 CLASS I, 15 CLASS II and 15 CLASS III sources were classified. Optical identification of the sample sources with USNO R magnitudes brighter than 17.0 corroborates with the results from the classification of the IR sources based on SED fitting. Among the sub-sample of 33 observed sources, 27 were found to present strong $H\alpha$ emission. However, 3 HAeBe, 1 CTTS and 13 WTTS are newly discovered.

The spatial distribution of the IR excessive emission sources selected based on their 2MASS colors reveals four sub-clusters toward IC 1396. One is spatially in association with the open cluster Trumpler 37 that hosts the exciting source of the H II region. The other three are found to be spatially coincident with the bright rims the surroundings. All the identified CLASS I and CLASS II sources are found to be located in the surrounding sub-clusters rather than the central young open cluster Tr 37, which is primarily a congregation of CLASS III sources. The surrounding sub-clusters are thus believed to much

younger due to the spatial distribution of IR sources at different evolutionary stages. This is consistent with a scenario of sequential star formation in this region. Imaging data of a dark patch in IC 1396 by Herschel SPIRE indicate the presence of two far-IR cores, which are likely evidence for new generations of star formation. Therefore, we infer that star formation in IC 1396 was not continuous but sequential and/or episodic.

Acknowledgements We appreciate very much the helpful comments and suggestions from the referee. This work employed data from the 2MASS, AKARI and other database. Our investigation is supported by funding from the National Natural Science Foundation of China through grant NSFC 11073027, 11003021 and the Department of International Cooperation of the Ministry of Science and Technology of China through grant 2010DFA02710.

References

- Barentsen, G., Vink, J. S., Drew, J. E., et al. 2011, *MNRAS*, 415, 103
- Bessell, M. S., & Brett, J. M. 1988, *PASP*, 100, 1134
- Choudhury, R., Mookerjee, B., & Bhatt, H. C. 2010, *ApJ*, 717, 1067
- Froebrich, D., & Scholz, A. 2003, *A&A*, 407, 207
- Froebrich, D., Scholz, A., Eisloffel, J., & Murphy, G. C. 2005, *A&A*, 432, 575
- Getman, K. V., Feigelson, E. D., Garmire, G., Broos, P., & Wang, J. 2007, *ApJ*, 654, 316
- Ishihara, D., et al. 2010, *A&A*, 514, A1
- Kawada, M., et al. 2007, *PASJ*, 59, 389
- Kun, M., Kiss, Z. T., & Balog, Z. 2008, in *Handbook of Star Forming Regions: The Northern Sky*, ed. B.Reipurth (San Francisco, CA: ASP), 136
- Lada, C. J. 1987, in *Proc. Symp. on Star Forming Regions*, Vol. 115, ed. M. Peimbert & J.Jugaku (Dordrecht: Reidel), 1
- Lada, C. J., & Adams, F. C. 1992, *ApJ*, 393, 278
- Lada, C. J., & Lada, E. A. 2003, *ARA&A*, 41, 57
- Li, J. Z., & Smith, M. D. 2005, *A&A*, 431, 925
- Lynds, B. T. 1962, *ApJS*, 7, 1
- Marschall, L. A., Karshner, G. B., & Comins, N. F. 1990, *AJ*, 99, 1536
- Martín, E. L. 1998, *AJ*, 115, 351
- Massey, P., Strobel, K., Barnes, J. V., & Anderson, E. 1988, *ApJ*, 328, 315
- Matthews, H. E., Haslam, C. G. T., Hills, D. L., & Salter, C. J. 1980, *A&A*, 88, 285
- Mercer, E. P., Miller, J. M., Calvet, N., et al. 2009, *AJ*, 138, 7
- Meyer, M. R., Calvet, N., & Hillenbrand, L. A. 1997, *AJ*, 114, 288
- Nakano, M., Sugitani, K., Watanabe, M., et al. 2012, *AJ*, 143, 61
- Neri, R., et al. 2007, *A&A*, 468, L33
- Onaka, T., et al. 2007, *PASJ*, 59, 401
- Patel, N. A., Goldsmith, P. F., Snell, R. L., Hezel, T., & Xie, T. 1995, *ApJ*, 447, 721
- Reach, W. T., et al. 2004, *ApJS*, 154, 385
- Reach, W. T., et al. 2009, *ApJ*, 690, 683
- Rieke, G. H., & Lebofsky, M. J. 1985, *ApJ*, 288, 618
- Robitaille, T. P., Whitney, B. A., Indebetouw, R., Wood, K., & Denzmore, P. 2006, *ApJS*, 167, 256
- Shu, F. H., Adams, F. C., & Lizano, S. 1987, *ARA&A*, 25, 23
- Sicilia-Aguilar, A., Hartmann, L. W., Hernández, J., Briceño, C., & Calvet, N. 2005, *AJ*, 130, 188
- Sicilia-Aguilar, A., Hartmann, L. W., Fürész, G., Henning, T., Dullemond, C., & Brandner, W. 2006, *AJ*, 132, 2135
- Simonson, S. C., III 1968, *ApJ*, 154, 923
- Sugitani, K., Fukui, Y., & Ogura, K. 1991, *ApJS*, 77, 59
- Weikard, H., Wouterloot, J. G. A., Castets, A., Winnewisser, G., & Sugitani, K. 1996, *A&A*, 309, 581
- Wendker, H. J., & Baars, J. W. M. 1980, *A&A*, 89, 180
- White, R. J., & Basri, G. 2003, *ApJ*, 582, 1109